In situ ground-based mobile measurement of lightning events above central Europe

Jakub Kákona[1], Jan Mikeš[1], Iva Ambrožová[2], Ondřej Ploc[2], Olena Velychko[2], Lembit Sihver[2,3], and Martin Kákona[2]

[1]Czech Technical University in Prague, Faculty of Electrical Engineering, Technická 2, 166 27 Prague, Czech Republic.
[2]Nuclear Physics Institute of the Czech Academy of Sciences, Husinec - Řež 130, 250 68 Řež, Czech Republic.
[3]Department of Radiation Physics, Atominstitut, Technische Universität Wien, Vienna, Austria.

Correspondence: Jakub Kákona (kakonjak@fel.cvut.cz)

Abstract. This article describes the equipment, and its advantages, used for in-situ ground measurements of thunderstorm phenomena using measuring cars. By using all-sky high-speed cameras, radio receivers, and electric field measurements, typical lightning discharges in the central Europe region have been characterized. Measurements of ionizing radiation during storms using a gamma spectrometer were also performed. At the ground level, no ionizing radiation originating in the storm cloud was detected even though during other experiments, using the same equipment at lower altitudes corresponding to the lower part of the storm clouds, ionizing radiation was detected. We showed that radio antennas with appropriately constructed receivers and all-sky high-speed cameras are devices that can significantly contribute to the understanding of processes taking place in the storm cloud during lightning discharges. On the contrary, measurements of the vertical electric field did not provide any new information about the processes occurring in the thunderclouds.

1 Introduction

The activity of storms is associated with many phenomena which nature is not yet fully understood or clarified. This includes the process of cloud electrification and the subsequent electric discharges, which are the most prominent manifestation of thunderstorms. As a result, forecasting and predictions of storm activity and related dangers are often very unreliable.

The storm activities are also associated with the generation of ionizing radiation. It is believed that this radiation is bremsstrahlung generated by electrons accelerated by an electric field in the thunderclouds. The electrons which are accelerated to relativistic velocities are called relativistic runaway electron avalanches (RREAs), which are then interacting with the atoms in the atmosphere (Dwyer, 2003; Gurevich et al., 1992). This causes a phenomenon that is often inaccurately called terrestrial gamma-ray flash (TGF) Fishman et al. (1994) or other phenomena like thunderstorm ground enhancement (TGE) (Chilingarian, 2013; Torii et al., 2002). Furthermore, there are experimental results showing that there are other ionizing radiation manifestations generated by storms. For example, there has been experimental evidence of the interaction of high-energy photons with the atmosphere causing nuclear reactions Enoto et al. (2017). The ionizing radiation that is thought to be associated with storm activity was measured using satellites in orbit around the Earth (e.g. Østgaard et al. (2019)), aircrafts flying inside or in the vicinity of storm clouds (Chilingarian et al., 2011; Kochkin et al., 2017; McCarthy and Parks, 1985; Parks et al., 1981) or high

mountain observatories e.g. (Chum et al., 2020; Tsuchiya et al., 2009). Currently, there are only a few measurements that could confirm the existence of ionizing radiation at lower altitudes, except for special storms that occur during the winter season in Japan, where storm clouds emerge low above the ground (Michimoto, 2007).

One of the most interesting measurements performed until now is the mapping of a radio signal emitted by lightning (Rison et al. (1999); Wu et al. (2018)). There exist TGF observations using ground detectors with simultaneous lightning mapping using radio signals Abbasi et al. (2018). Despite these very detailed observations, the exact location of the source of the ionizing radiation within the storm cloud remains unknown Belz et al. (2020). Moreover, the TGFs have only rarely successfully been measured at the ground level (Kereszy et al., 2022; Rakov and Kereszy, 2022; Dwyer et al., 2012; Wada et al., 2019).

To be able to measure different processes which occur during thunderstorms, we equipped cars with measuring equipment. These cars are able to move to locations with a predicted storm activity and thus react to specific storm developments, and perform ground measurements directly at the storm site.

During the 2021 summer storm season, we carried out many expeditions in the Czech Republic and Slovakia with the equipment described in detail below. This allowed us to measure the electrostatic, magnetic, electromagnetic, and optical properties of storms, including ionizing radiation. In this paper, we present the results of these measurements and how we characterized the recorded lightning, especially the lengths of their duration. We relate optical observations with measurements of electromagnetic radiation in the radio spectrum, and with changes in electric and magnetic fields at the measuring site. Thanks to the comparison of different obtained lightning recordings with each other we are able to reconstruct the individual phases of lighting in the optical spectrum.

2 Measuring equipment

In order to determine the necessary parameters of lightning activity (lightning events' timestamps, lightning type, and location), we equipped the two measuring cars see Fig. 1 (CAR0 and CAR1) with high-speed all-sky cameras and radio receivers. The cars were used to transport and power the instruments in the proximity of thunderstorms. The car cabin also served as partial protection for instrument operators.

2.1 High-speed all-sky Cameras

Chronos 1.4 camera CR14-1.0-16M KronTechInc. (2021) is mounted in a waterproof SolidBox 69200. The box is covered with a plexiglass dome with the manufacturer designation Duradom 200mm depicted in Fig. 2.

The video resolution of the camera is 928x928 pixels with 1612.33 FPS and a constant shutter in the range of 4.9 to 34 µs during daytime thunderstorms and maximal time 614.6 µs for nighttime thunderstorms. The shutter time is set by the instrument operator depending on current weather conditions. The video-saving length of the camera was set to 2 or 3 seconds. The video save format is H.264 resulting in MPEG-4 (.mp4) video, which sacrifices a bit of the quality for better compression. The main possible loss is gamma-encoded brightness, which possibly alters the absolute values of the real brightness of recorded lightning.

Figure 1. Measuring CAR0 with instruments mounted on the roof platform.

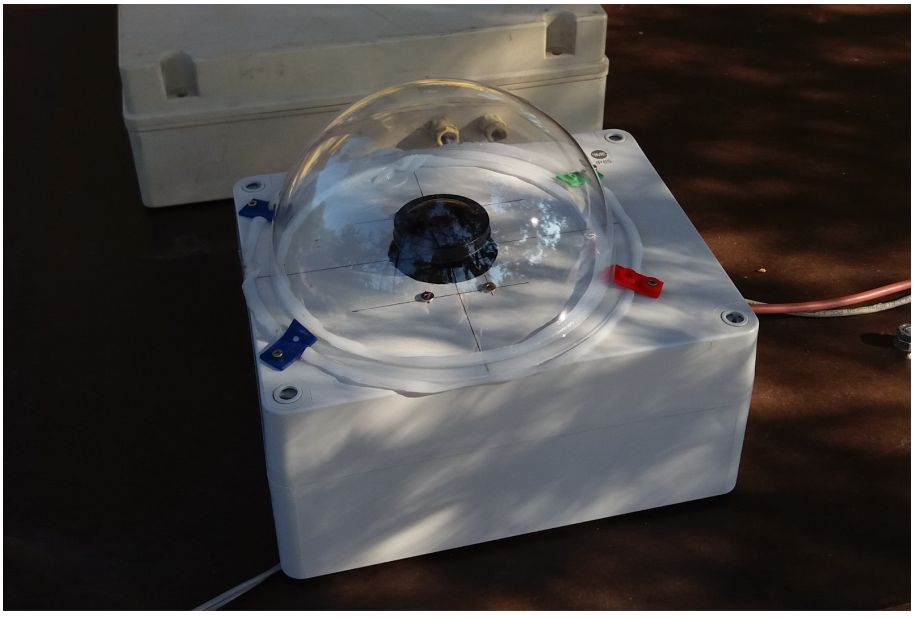

Figure 2. The camera has a wide-angle CS camera lens and is equipped with an IR-blocking filter mounted in front of the LUX1310 CMOS sensor.

The camera lenses we used were FE185C057HA-1 Fujifilm (2021). The high-speed camera was therefore only sensitive to visible light. This spectral baseband was selected to minimize the absorption of light generated by lightning in the atmosphere.

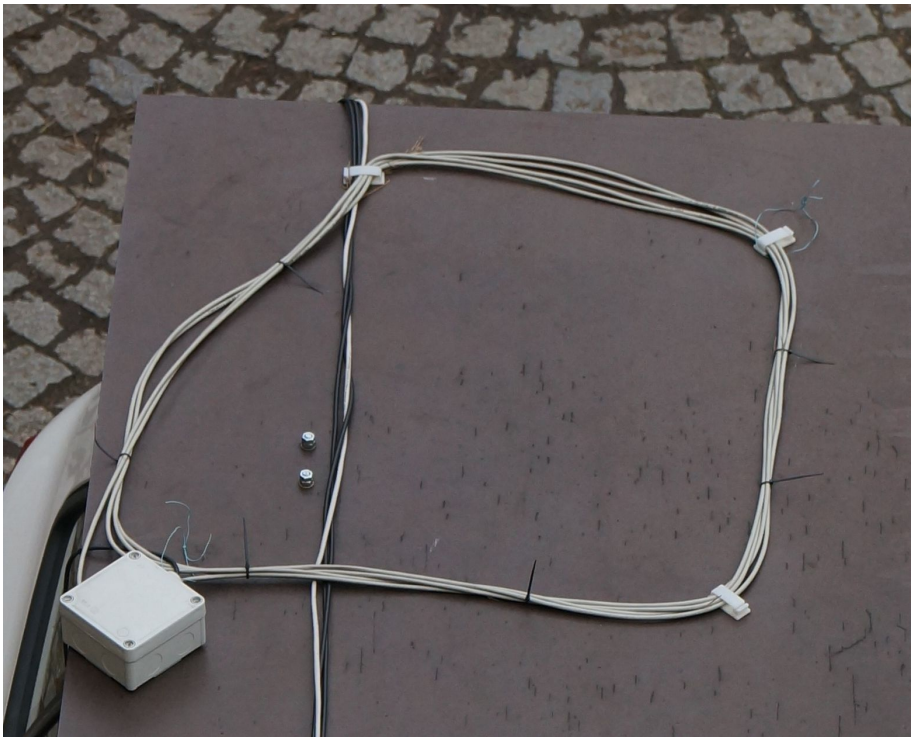

Figure 3. The STP loop antenna mounted on the measuring car CAR1 has a resonant frequency of 100 kHz. Its signal was directly sampled by an oscilloscope placed inside the car.

2.2 Radiofrequency receivers

Different radio frequency receivers were used to record the radio emissions generated by lightning activities. The main objective was to cover a wide radio frequency band. The VLF radio frequency band is known to be sensitive mainly to large-size and high-current lightning channels, such as the return stroke. On the contrary, the UHF radio frequency band involves radiation almost exclusively associated with the fine structure of lightning Shi et al. (2019).

2.2.1 VLF signal receiver

The VLF signal receiver is based on a magnetic loop antenna and storage oscilloscope with a control computer for data readout. For one lightning event, we could record 800 ms of 8bit samples with a sampling rate of 250 $\mathrm{MS/s}$.

The antenna design was based on the use of VLFANT01 MLAB.cz (2017) module, with the 10 m length, STP cable coiled into four loops (STP antenna). The STP antenna loop was placed horizontally directly at the plywood base mounted on the car roof. See Fig. 3 for details.

This VLF receiver system was also used for detection of the lightning and triggering other instruments in the cars. The detection of the lightning was based on pulse width and the signal level; both parameters were set by the operator during the

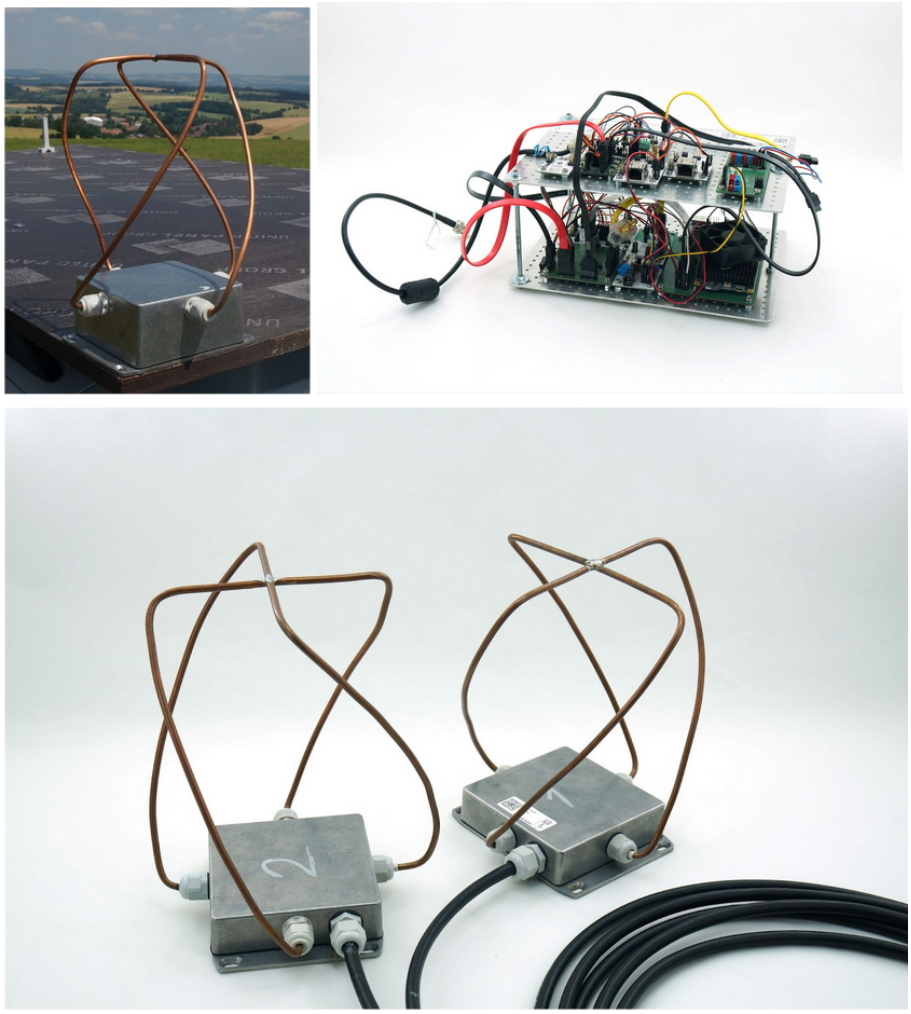

Figure 4. The platform of a QFH receiver antenna is shown in the top left corner. Detailed pictures of the antenna can be seen at the bottom and the receiver is shown at the top right.

thunderstorm event. The range of these parameters is usually 5 to 20 µs for the pulse width and 10 to 30 mV for the signal level. An example of the measured signal can be seen in ~~Fig. 11~~section 4.3.

2.2.2 UHF signal receiver

The UHF receiver operates approximately in the 370-406 MHz band, exact tuning depends on the local noise within the 10 MHz receiver bandwidth. The signal is received by an array of four QFH antennas mounted in a square-like configuration on the roof platform of the measuring car as is shown in the photos in Fig. 4 and 1. The signal from each antenna is directly

downconverted by an RF mixer to I and Q analog channels. Each channel is sampled by a 12bit analog to digital converter with 10 $\mathrm{MS/s}$.

The construction of the receiver itself is designed in a way that enables a phase processing of the signal from the antenna array with the aim of detailed mapping of the discharge UST.cz (2021). However, in the case of this experiment, only the scalar envelope of the radio signal is considered. The block diagram of the receiver is shown in Appendix Figure A1.

The radio receiver, in the case of an external trigger, records a section of the configurable length of pre-trigger and post-trigger blocks which are up to 1.45 seconds long. The radio signal is simultaneously sampled from the whole antenna array. This feature is achieved by using a ring buffer that stores the samples before the trigger. Thanks to a PPS signal from an external GNSS receiver, the resulting recorded file at the same time contains the sub-microsecond absolute time of each recorded sample.

The antennas are mounted on an electrically non-conductive 18 mm thick plywood board (identical to CAR 1 with VLF receiver) attached to the roof of the measuring car by crossbars, located above the car's metal roof.

The construction of a single antenna array element is based on the quadrifilar helix design. The antenna contains two loops, which are joined together on one side and connected to the active analog fronted PCB of the antenna (QFHMIX01) on the other side. QFHMIX01 PCB is mounted in a metal enclosure. The antenna half-loops pass through the enclosure wall by waterproof cable glands. Each joint of the half-loop and QFHMIX01 PCB is considered a 40 Ω port. The signal on each port has a 90° signal phase shift in relation to the next port. That feature allows the processing of the signal from the antenna as quadrature I/Q data, which significantly increases the capabilities of subsequent signal processing.

2.3 Ionizing radiation detectors

During the whole measuring campaign, NaI(Tl) ionizing radiation detector and Silicon Photomultiplier (SiPM) sensors were used. The details about the used gamma spectrometer AIRDOS-C can be read in Velychko et al. (2022). The energy deposition range of this device is 200 keV to 40 MeV. The time resolution between two incident ionizing radiation events is 100 µs for particles with deposited energy above 1 MeV. For lower energies, only 15 s integration of events is provided. The NaI(Tl) crystal with SiPM and preamplifier is shielded in a metallic box.

2.4 Electric Field Mill

The electric field is measured using the Electric Field Mill (EFM) Kleinwächter EFM 115 from which the analog signal output leads directly to the data logger that contains a GPS receiver for the timestamping of the record MLAB.cz (2021). The time resolution of the logging is 110 ms.

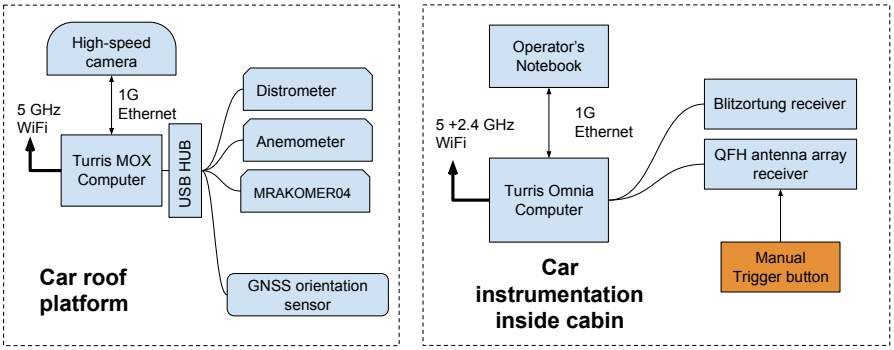

Figure 5. CRREAT CAR0 instrumentation schematic diagram.

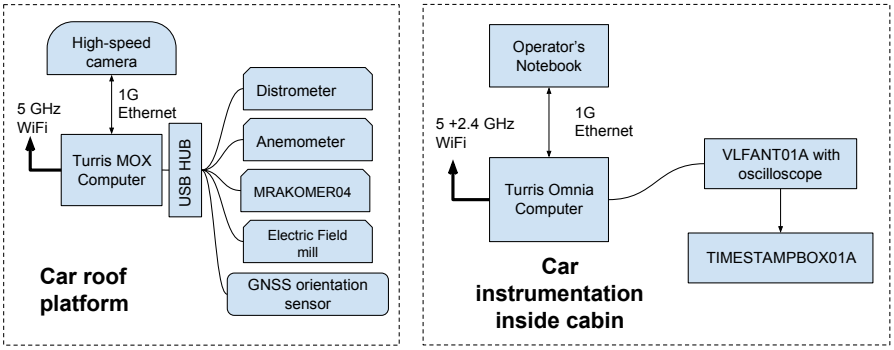

Figure 6. CRREAT CAR1 instrumentation schematic diagram.

2.5 Meteorological instruments

In order to determine the meteorological situation in the vicinity of the car during the measurement, the car is equipped with several meteorological sensors: a distrometer UST.cz (2020), an anemometer MLAB.cz (2020) and a thermometer with a barometer MLAB.cz (2015).

3 Observation methods

Observations were carried out with a gradually improved strategy with the aim of getting the measuring cars (especially the one equipped with radiation detectors) as close to the storm center as possible. The position of the storm center was monitored using data from third-party networks Windy (Windyty, 2021), Blitzortung.org (Egon Wanke, 2011).

The position of the measuring car was stationary during the measurements of the thunderstorms. Moreover, in the case of radiation detectors, an extended static position time interval was used before and after storm activity in order to be able to record the whole development of radiation change including the local parameters of the radiation background.

During the measuring campaigns, the method of data recording developed as well. During the first campaigns, we were trying to make automatic recordings based on observed electromagnetic signals. This system however had a lot of imperfections leading to its abandonment in the measuring car CAR0, where it was replaced by manual activation of recording. See the Fig. 5. The manual activation of the recording was based on the visual perception of the operator observing the lightning activity. In contrast to CAR0, CAR1 was left with a semi-automatic method of activating the recording for the purpose of comparing the efficiency of both trigger methods. Car CAR1 thus had a recording trigger based on using a loop antenna and oscilloscope that generated triggers for other devices based on amplitude measurements and a length of voltage pulse on antenna output. See the Fig. 6. The trigger signal was distributed via the Ethernet network, a solution common to both measuring cars.

During the observation itself, a significant problem was caused by the time needed to record the data measured by individual detectors resulting from the time period needed to store the recording from the operational memory of devices. We were able to reduce the time mainly by optimizing the camera settings and using different firmware. Nevertheless, the total dead time was still about 90 seconds in case of storms occurring during the day. In the case of night storms, the dead time decreased to approximately 60 seconds due to the image compression used. As a consequence, all lightning events were not recorded for any storm event.

4 Results

4.1 Ionizing radiation measurements

Figure 7 shows an example of ionizing radiation measurement using the gamma spectrometer AIRDOS-C. In the upper graph, a storm approaching a parked measuring car is displayed using data from the Blitzortung.org network. The vertical red lines mark the times when lightning was registered by the STP antenna. The lower graph shows the number of particles registered by the ionizing radiation detector every 15 seconds. In this particular example, the lightning activity ceased just after 20:30. The graph shows an increase in ionizing radiation flux by approximately 30 %. This increase is related to a radon progenies washout from the atmosphere caused by rain that started at 19:45.

Figure 8 shows a short time period of the ionizing radiation measurement at the time when the storm was closest to the car. Individual particles of ionizing radiation registered versus detected lightning are shown. Only particles that have passed on energies higher than 2.4 MeV to the detector are displayed.

4.2 Camera measurements

During the measurement, the camera is pointed toward the zenith and its lens allows it to capture the entire sky from horizon to horizon. For the illustration of the camera view, a plain camera frame is shown in Fig. 9. Because lightning discharges often happen inside clouds, and lightning channels are not directly visible, we converted the videos of the recorded lightning to luminosity in time. The integral values of the illuminations were calculated by a script from the video recordings of high-speed

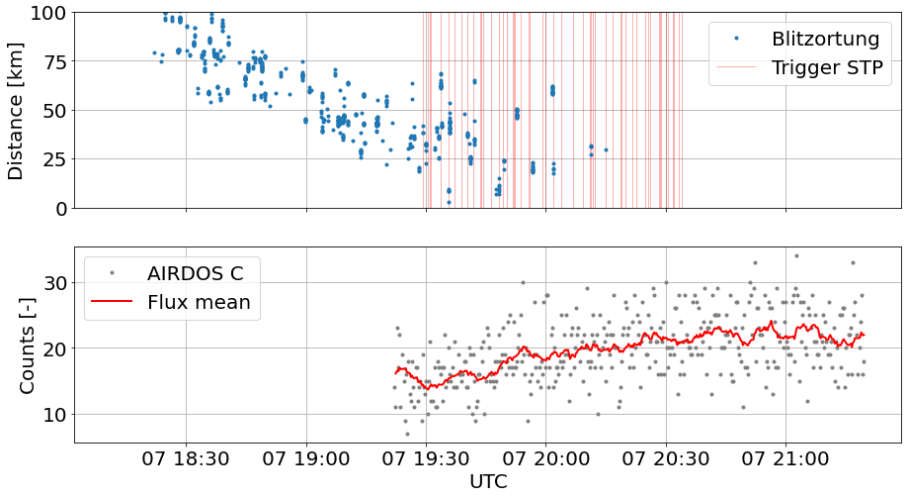

Figure 7. Measurements of ionizing radiation using a car compared to lightning registered by antennas. The beginning of the measurements using AIRDOS-C and STP antennas corresponds to switching on the devices after parking the car on a spot at 19:15. The measurement ended at 21:25 by switching off the devices and leaving the measuring spot.

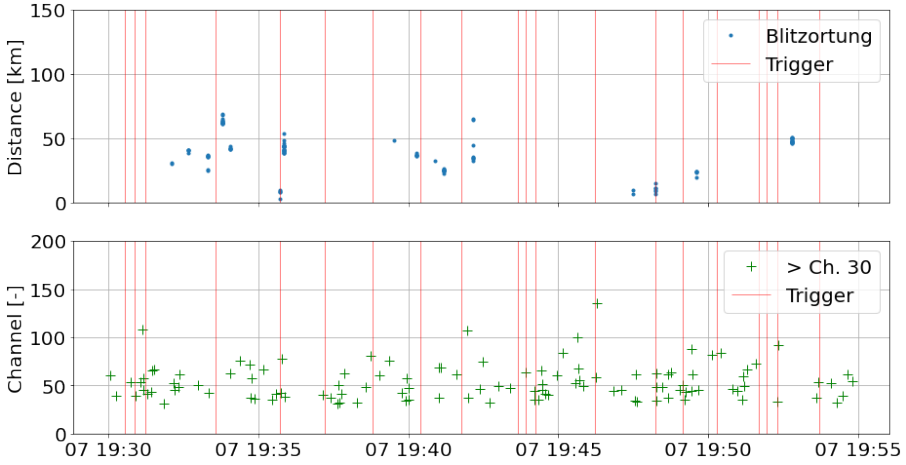

Figure 8. Lightning detected by Blitzortung.org and triggers from STP antenna plotted together with individual registered particles of ionizing radiation above channel 30 of gamma spectrometer.

cameras. The calculations were carried out over the entire image area by summing up the values of all pixels on each image. We call these luminosity curves. The results can be seen on graphs in Fig. 10 depicting the course of light flux over time.

To maintain clarity, luminosity curves were added to videos, which were converted from BW recordings captured by cameras to false colors in order to make details of lightning (that have high luminosity dynamics) visible.

Figure 9. A still image example from the all-sky camera showing the horizon and the fish-eye lens distortion.

The following enclosed video [1627302288.9546976.mp4] shows very well a flash of lightning together with leaders and recoil leaders. During the ~~measurement, the camera is pointed toward the zenith and its lens allows it to capture the entire sky from horizon to horizon. For the illustration of the camera view, a plain camera frame is shown in Fig. 9. During the~~ thunderstorm recording, the camera gain was decreased in order to capture lightning that has high brightness dynamics. As a result, lightning is not visible in the video together with details of clouds and surrounding terrain. The processed video has the position of the horizon marked with a green circle with an inscribed designation of the cardinal directions. In the upper part of the video, there is a white graph showing the luminosity curve with a green pointer marking showing the position of the current frame over time. On the right a color palette is visible, corresponding to the brightness recorded by each camera pixel with a depth of 8 bits. The bottom line shows the number of the current frame over the total number of frames recorded. The next is Sg=1/1 (information which part of the camera's internal memory was used for recording) and the time of the current frame 'T=' in seconds relative to the trigger.

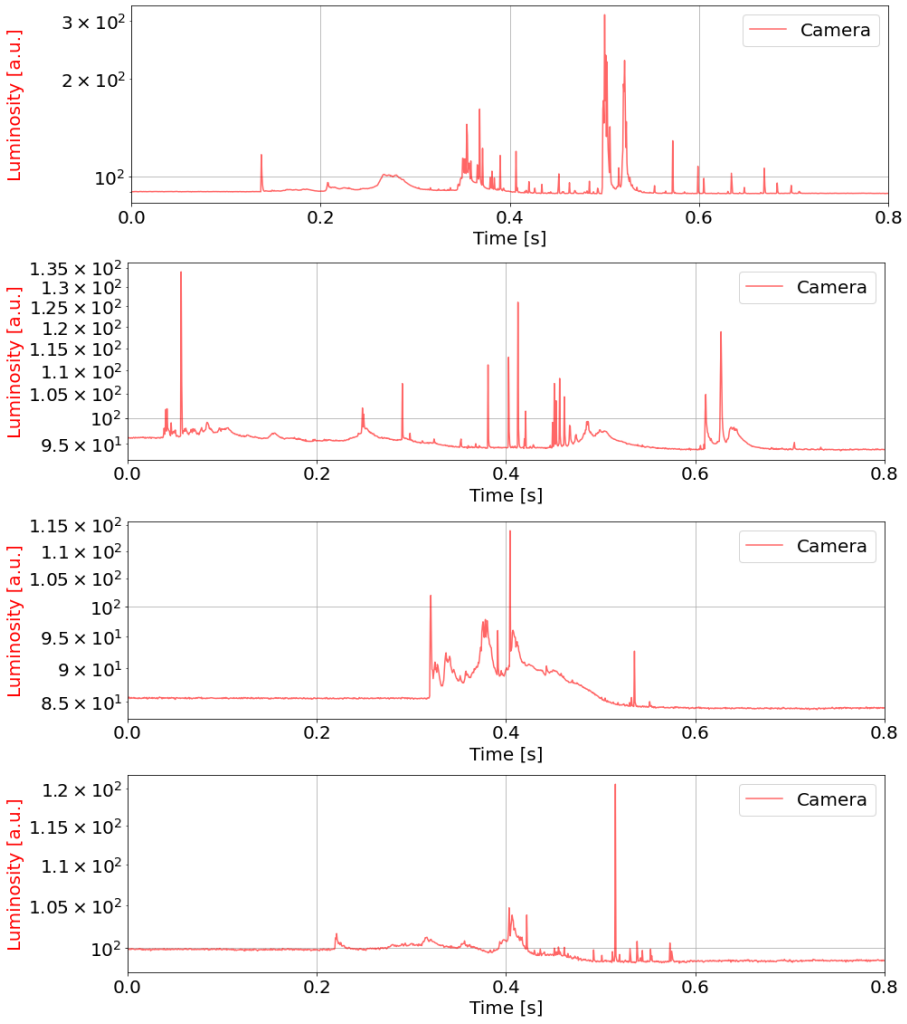

Figure 10. An example of luminosity curves for a few lightning.

The resulting luminosity curves contain similar parts (sharp peaks or slow changes of luminosity). Thanks to this, we can compare the video recordings of luminosity curves with a similar progression, and from several recordings, we can choose those parts that have similar luminosity curves and a visible lightning channel (not covered by clouds). Such a process helps us to see what lightning really looks like.

4.3 Antenna measurements

One of the advantages of measuring lightning using magnetic loop antennas is that the observation is not disturbed by optically non-transparent clouds or, as is the case of storms occurring during the day, sunlight scattered in the atmosphere. On the other hand, when we use a coil to measure the magnetic component of the electric field, we only see its changes in time or specifically

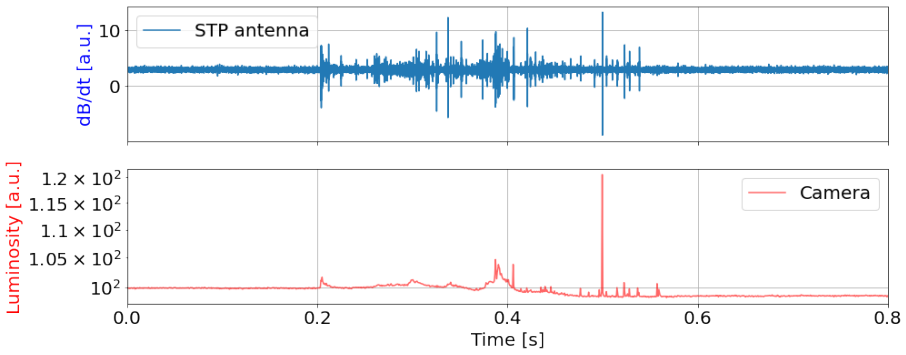

Figure 11. Example of data from STP antenna with the comparison to camera data.

a change in the current that flows through the lightning channel. If a constant current flows through the lightning channel it is not possible to detect it using a magnetic loop antenna. Figure 11 shows an example of lightning recorded by an STP antenna and a camera at the same time. In the camera recording, a change in light conditions is clearly visible. The sky was brighter before the lightning than after it occurred. Slow changes in brightness, and thus slow changes in current, are not visible on the antenna recording. On the other hand, we see clusters of fast pulses that can give information about the development of lightning channels, which are not visible on the camera recordings because they are probably obscured by light emanated by a constant current in the main channel. Pulses, visible on both camera and antenna recordings are recoil leaders. The most prominent pulse is the CG return stroke.

4.4 Correlation of measured lightning with lightning detection network

We have tried to compare the detection of lightning using the STP antenna with its detection using the Blitzortung.org network. First, we have to note that not every lightning detected by the STP antenna was recorded, because it takes several minutes to store the data of every lightning from an oscilloscope to the data storage. Second, not every lightning detected by the STP antenna is detected by the Blitzortung.org network. Figure ~~13~~ 12 shows that at the point when the storm was closest to the car according to the Blitzortung.org network the STP antenna detected lightning at a different time or distance of more than 120 km. On the contrary, as shown in Fig. ~~12~~13, when according to the Blitzortung.org network the storm was located tenths of kilometers away from the observation site we see perfect conformity to the data from the STP antenna. In both figures, an interval of ± 1 s is marked around the vertical lines corresponding to the detection times.

Lightning at 18:24:48 was detected by a high-speed camera, see video [1627302288.9546976.mp4]. According to the video, one of the lightning channels occurred almost directly above the measurement car but the nearest lightning detected by Blitzortung.org was at least 70 km away. The positioning accuracy in the case of the Blitzortung.org network is in the order of kilometers. Blitzorting.org detected discharges at a distance from 70 to 80 km simultaneously. That's why we can deduce that this lightning was more than 80 km long or there occurred a synchronous discharge 80 km away.

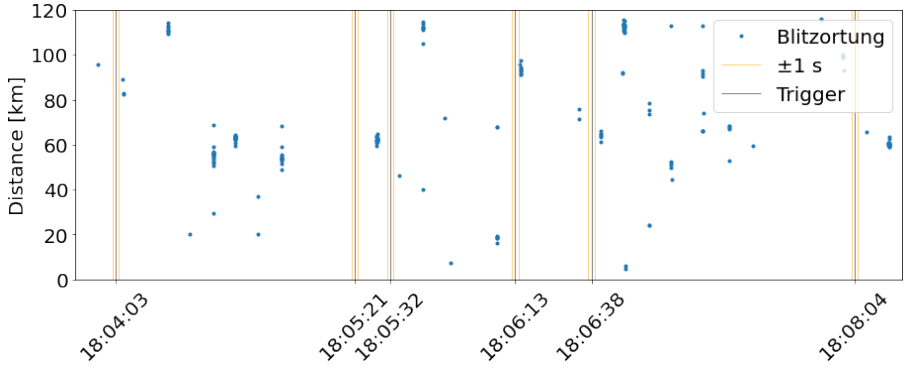

Figure 12. Correlation with "nearby" (less than 20 km) lightning detection.

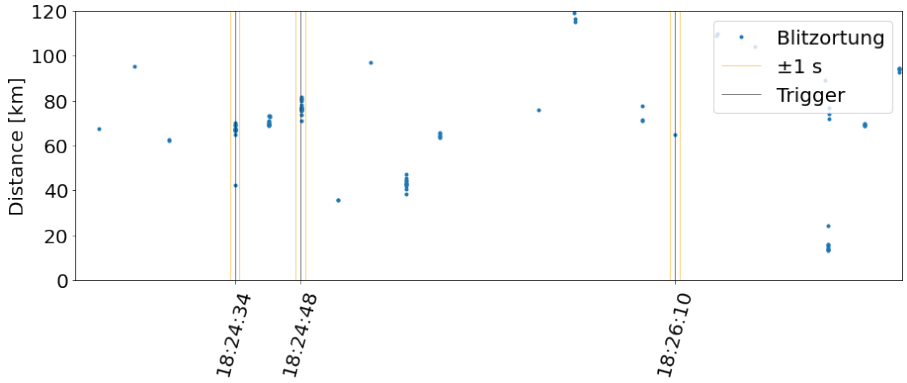

Figure 13. Correlation with "distant" (more than 40 km) lightning detection.

4.5 Electric field measurements

Figures 14 and 15 show a comparison of the vertical electric field measurements at the car measuring site with the camera recordings. The EFM on the car is not grounded and thus it measures the gradient of the electric potential between the sensor and the car body. As can be seen in Fig. 14 the electric discharges occur at times of large electric field changes. If we, however, look at the details of some discharges recorded by the camera (Fig. 15) we can find out that the changes in the electric field do not correspond directly to individual discharges. Please note that EFM measures the vertical component of the electric field, which gives the integrated value over a large area of clouds and the field is also deformed by the presence of a car.

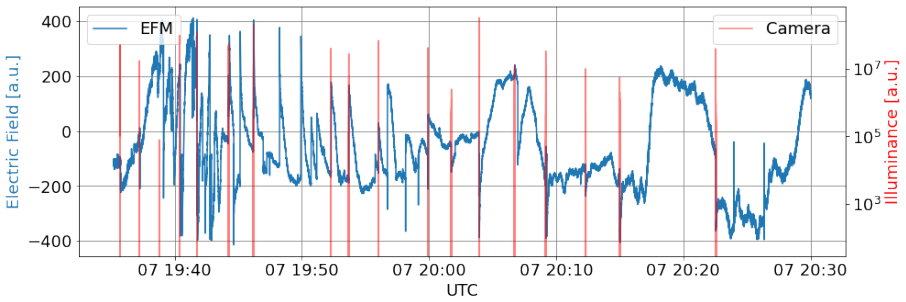

Figure 14. Example of measurement with EFM compared with records of lightning captured on the camera.

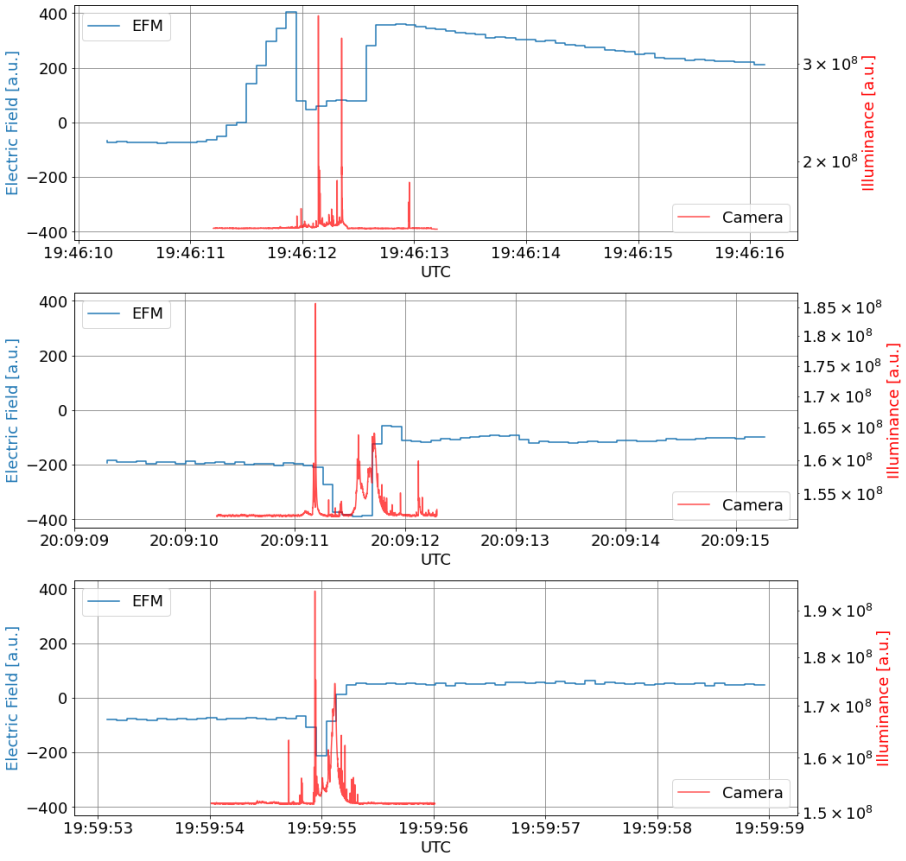

Figure 15. Detail of EFM data with a comparison with camera data.

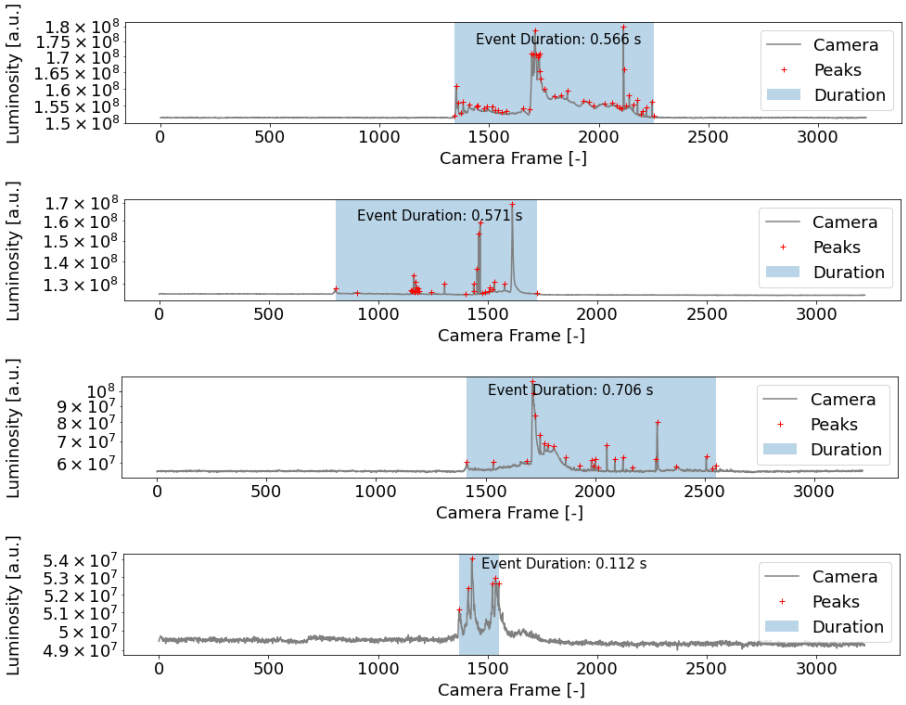

Figure 16. Examples of detection of lightning events duration. Red crosses are detected peaks in signals generated by lightning processes. The determined length of lightning duration is highlighted. The duration of the camera frame is 620 µs.

5 Discussion

5.1 Lightning duration

We were searching for the duration of the lightning event by searching for local maxima of illumination of the camera chip in time from peaks that have a prominence higher than two times of noise. Then the first and last maxima were used for the determination of the first and last snap and from the framerate the lightning duration was calculated. First, ten snaps of the camera record were omitted because of possible artifacts of used video data compression. The amplitude of noise was established from the first 100 frames (from frame 10 to frame 110). Examples of how we determined the duration of some lightning are shown in Fig. 16 and 17. The histogram of durations of lightning events is shown in Fig. 18. This histogram comprises 107 lightning events measured during 12 thunderstorms.

To calculate the total length of a lightning event from a radio signal shown in Fig. 17, we use a methodology that treats signals greater than 4σ variance, calculated from the moving window of 10 ms, to be the start of the lightning discharge. This algorithm is applied symmetrically from both ends of the recorded signal. Therefore, the recording of the length of the lightning begins from the first sample of the detected signal and ends from the last sample of the recorded signal.

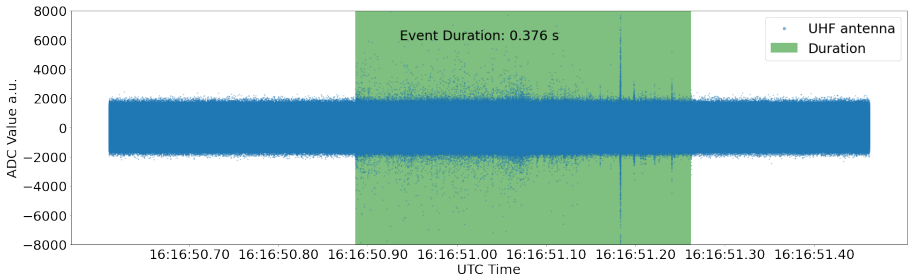

Figure 17. Example of lightning duration measurement based on radio signals captured by the UHF receiver. The time duration of lightning is marked by the green overlay.

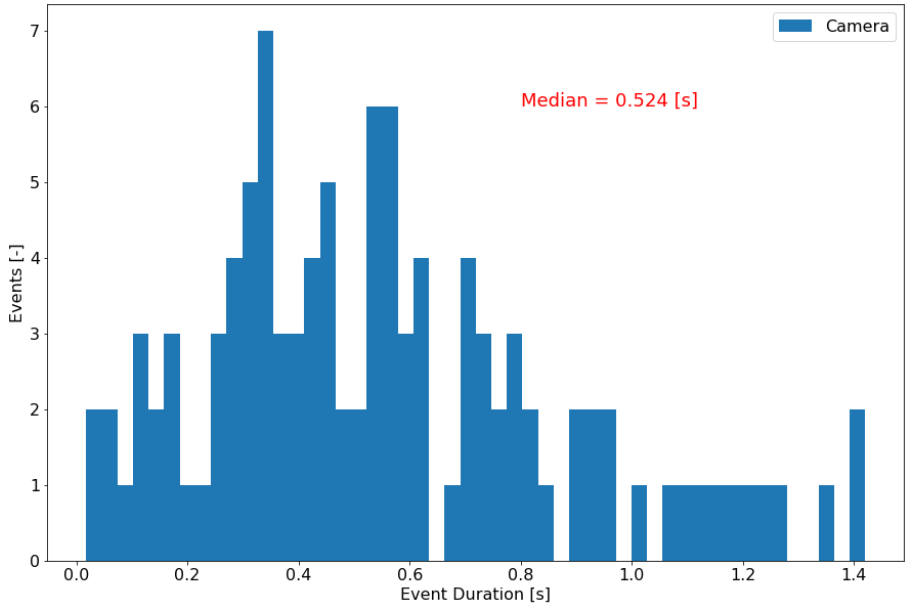

Figure 18. Histogram of the observed duration of lightning events. The histogram is based on data captured by the high-speed cameras.

The measured durations are usually in the order of hundreds of milliseconds, only exceptionally there are shorter lightning events. The median duration of lightning events is 524 ms. This result is significantly longer than was mentioned in previous studies 200-300 ms Rakov and Uman (2003) and 350 ms López et al. (2017).

The processing of lightning recordings differs for day and night storm observations, as they require different settings of the high-speed camera. In particular, the setting of the exposition lengths and the analog gain varies. This difference could affect the exact measurements of the total length of a discharge, resulting in a shortening of the estimated time duration. Because of sunlight scattered in the atmosphere during the daytime, the weak discharges might have been omitted. Therefore the extracted time durations of lightning events could be underestimated.

From the following analysis of the lightning duration, we excluded two thunderstorms where it was not possible to distinguish between individual lightning events, which means events for which there were less than 500 ms between the individual detected discharges. We consider lightning to be an event where the time between the individual discharges does not exceed 100 ms.

5.2 Lightning development/characterization

Data from cameras reveal similar phases of lightning development. We provide examples of video recordings with individual phases clearly visible and unobscured by clouds.

Video [1627302745.846055.mp4] captures (from T=+0.27 s (1:11) to T=+0.40 s (1:22)) a positive side of leader. When the current flowing through the leader begins to weaken, recoil leaders start to appear at its end (T=+0.38 s (1:21)). The term recoil leader was taken from literature Mazur et al. (2013). Based on our observations, however, we cannot confirm that all the visible recoil leaders reuse an already-established ionized channel.

Video [2021-08-15-20-07-35.912167-lightning.mp4] captures an invisible positive leader, only blurred recoil leaders are visible. From T=+0.07 s (1:36) a negative side of leader is visible. Negative leader branches abundantly, its propagation is faster than the positive leader and contains hot luminous ends. The second visible negative leader starts at T=+0.25 s (1:51). The negative leaders do not generate recoil leaders.

Based on the experience from the recordings, in which some parts of the lightning are clearly visible, we can characterize other lightning events. In Fig. 11, an example of the luminosity curve and antenna data is shown. At the very beginning, the lightning usually starts with a faith peak with a fast-rising edge (at the time 0.2 s). Then there is an optically dark phase with low luminosity. This quiet period is not really quiet in the radio signal. It is a phase of developing a leader. As the leader in the cloud connects to more and more charged regions it becomes brighter, sometimes slowly sometimes abruptly. During and after a decrease in the current in the positive leader, the recoil leaders are appearing (after the time 0.4 s). Some recoil leaders have high luminosity when they connect to the main channel. In the radio spectrum, we simultaneously observe peaks that correspond to short intense brightenings. In some cases the lightning results in CG discharge, which is accompanied by high-intensity flash (at the time 0.5 s). However, this phenomenon does not occur very often. Using the described equipment we registered CG return strokes in less than 10 % of cases.

6 Conclusions

During the 2021 summer storm season, we collected data on more than 100 lightning events using cars equipped with all-sky high-speed cameras, radio receivers, and electric field detectors. We conclude, based on the experience from these measurements, that the data from all-sky high-speed cameras and magnetic, or electromagnetic antennas, give comparable results in terms of lightning durations. The median duration of the measured lightning is 0.52 s, which is longer than what is stated in the literature. We have shown that the data obtained by EFM (measurement of the vertical electric field) do not provide any new information about the development of lightning. We were also not able to prove a direct connection between the increase

in ionizing radiation and lightning in the lowlands of Central Europe. During further experiments, we want to focus on the triangulation of the discharges, using antennas and cameras simultaneously, so that the actual dimensions of lightning and the distance from lightning can be determined. We want to concentrate on measuring the electric field in the horizontal plane at the altitude of the thundercloud base. We believe that these measurements could contribute to a better understanding of where and when the ionizing radiation originates in thunderstorms.

Data availability.

All raw data can be provided by the corresponding authors upon request.

Appendix A

Author contributions.

JK, MK planned the campaign and performed the measurements; MK, JK, and OV analyzed the data; MK and JK wrote the manuscript draft; IA, OP, LS, and JM reviewed and edited the manuscript.

Competing interests.

The authors declare that they have no conflict of interest.

Acknowledgements. This work was supported by EU Operational Program Research, Development, and Education in project CRREAT (Research Center of Cosmic Rays and Radiation Events in the Atmosphere) [CZ.02.1.01/0.0/0.0/15_003/0000481].

References

Abbasi, R. U., Abu-Zayyad, T., Allen, M., Barcikowski, E., Belz, J. W., Bergman, D. R., Blake, S. A., Byrne, M., Cady, R., Cheon, B. G., Chiba, J., Chikawa, M., Fujii, T., Fukushima, M., Furlich, G., Goto, T., Hanlon, W., Hayashi, Y., Hayashida, N., Hibino, K., and Zundel, Z.: Gamma ray showers observed at ground level in coincidence with downward lightning leaders, Journal of Geophysical Research: Atmospheres, 123, 6864–6879, https://doi.org/10.1029/2017JD027931, 2018.

Belz, J. W., Krehbiel, P. R., Remington, J., Stanley, M. A., Abbasi, R. U., LeVon, R., Rison, W., Rodeheffer, D., Abu-Zayyad, T., Allen, M., Barcikowski, E., Bergman, D. R., Blake, S. A., Byrne, M., Cady, R., Cheon, B. G., Chikawa, M., di Matteo, A., Fujii, T., Fujita, K., Fujiwara, R., Fukushima, M., Furlich, G., Hanlon, W., Hayashi, M., Hayashi, Y., Hayashida, N., Hibino, K., Honda, K., Ikeda, D., Inadomi, T., Inoue, N., Ishii, T., Ito, H., Ivanov, D., Iwakura, H., Jeong, H. M., Jeong, S., Jui, C. C. H., Kadota, K., Kakimoto, F., Kalashev, O., Kasahara, K., Kasami, S., Kawai, H., Kawakami, S., Kawata, K., Kido, E., Kim, H. B., Kim, J. H., Kim, J. H., Kuzmin†, V., Kuznetsov, M., Kwon, Y. J., Lee, K. H., Lubsandorzhiev, B., Lundquist, J. P., Machida, K., Matsumiya, H., Matthews, J. N., Matuyama, T., Mayta, R., Minamino, M., Mukai, K., Myers, I., Nagataki, S., Nakai, K., Nakamura, R., Nakamura, T., Nakamura, Y., Nonaka, T., Oda, H., Ogio, S., Ohnishi, M., Ohoka, H., Oku, Y., Okuda, T., Omura, Y., Ono, M., Oshima, A., Ozawa, S., Park, I. H., Potts, M., Pshirkov, M. S., Rodriguez, D. C., Rubtsov, G., Ryu, D., Sagawa, H., Sahara, R., Saito, K., Saito, Y., Sakaki, N., Sako, T., Sakurai, N., Sano, K., Seki, T., Sekino, K., Shibata, F., Shibata, T., Shimodaira, H., Shin, B. K., Shin, H. S., Smith, J. D., Sokolsky, P., Sone, N., Stokes, B. T., Stroman, T. A., Takagi, Y., Takahashi, Y., Takeda, M., Takeishi, R., Taketa, A., Takita, M., Tameda, Y., Tanaka, K., Tanaka, M., Tanoue, Y., Thomas, S. B., Thomson, G. B., Tinyakov, P., Tkachev, I., Tokuno, H., Tomida, T., Troitsky, S., Tsunesada, Y., Uchihori, Y., Udo, S., Uehama, T., Urban, F., Wallace, M., Wong, T., Yamamoto, M., Yamaoka, H., Yamazaki, K., Yashiro, K., Yosei, M., Yoshii, H., Zhezher, Y., and Zundel, Z.: Observations of the Origin of Downward Terrestrial Gamma-Ray Flashes, Journal of Geophysical Research: Atmospheres, 125, e2019JD031 940, https://doi.org/https://doi.org/10.1029/2019JD031940, e2019JD031940 10.1029/2019JD031940, 2020.

Chilingarian, A.: Thunderstorm Ground Enhancements (TGEs) – New High-Energy Phenomenon Originated in the Terrestrial Atmosphere, Journal of Physics: Conference Series, 409, 012 019, https://doi.org/10.1088/1742-6596/409/1/012019, 2013.

Chilingarian, A., Hovsepyan, G., and Hovhannisyan, A.: Particle bursts from thunderclouds: Natural particle accelerators above our heads, Physical Review D, 83, 062 001, https://doi.org/10.1103/PhysRevD.83.062001, 2011.

Chum, J., Langer, R., Baše, J., Kollárik, M., Strhárský, I., Diendorfer, G., and Rusz, J.: Significant enhancements of secondary cosmic rays and electric field at the high mountain peak of Lomnický Štít in High Tatras during thunderstorms, Earth, planets, and space: EPS, 72, 28, https://doi.org/10.1186/s40623-020-01155-9, 2020.

Dwyer, J. R.: A fundamental limit on electric fields in air, Geophysical Research Letters, 30, https://doi.org/10.1029/2003GL017781, 2003.

Dwyer, J. R., Schaal, M. M., Cramer, E., Arabshahi, S., Liu, N., Rassoul, H. K., Hill, J. D., Jordan, D. M., and Uman, M. A.: Observation of a gamma-ray flash at ground level in association with a cloud-to-ground lightning return stroke, Journal of Geophysical Research: Space Physics, 117, https://doi.org/https://doi.org/10.1029/2012JA017810, 2012.

Egon Wanke: Blitzortung.org - A low cost Time of Arrival Lightning Detection and Lightning Location Network, accessed 19 February 2022, https://www.blitzortung.org/Documents/TOA_Blitzortung.pdf, 2011.

Enoto, T., Wada, Y., Furuta, Y., Nakazawa, K., Yuasa, T., Okuda, K., Makishima, K., Sato, M., Sato, Y., Nakano, T., Umemoto, D., and Tsuchiya, H.: Photonuclear reactions triggered by lightning discharge., Nature, 551, 481–484, https://doi.org/10.1038/nature24630, 2017.

Fishman, G. J., Bhat, P. N., Mallozzi, R., Horack, J. M., Koshut, T., Kouveliotou, C., Pendleton, G. N., Meegan, C. A., Wilson, R. B., Paciesas, W. S., Goodman, S. J., and Christian, H. J.: Discovery of intense gamma-ray flashes of atmospheric origin., Science, 264, 1313–1316, https://doi.org/10.1126/science.264.5163.1313, 1994.

Fujifilm: FE185 Series, Super wide-angle lenses, accessed 13 April 2022, https://www.fujifilm.com/us/en/business/optical-devices/machine-vision-lens/fe185-series, 2021.

Gurevich, A. V., Milikh, G. M., and Roussel-Dupre, R.: Runaway electron mechanism of air breakdown and preconditioning during a thunderstorm, Physics Letters A, 165, 463–468, https://doi.org/10.1016/0375-9601(92)90348-P, 1992.

Kereszy, I., Rakov, V. A., Ding, Z., and Dwyer, J. R.: Ground-Based Observation of a TGF Occurring Between Opposite Polarity Strokes of a Bipolar Cloud-To-Ground Lightning Flash, Journal of Geophysical Research: Atmospheres, 127, e2021JD036 130, https://doi.org/https://doi.org/10.1029/2021JD036130, e2021JD036130 2021JD036130, 2022.

Kochkin, P., van Deursen, A. P. J., Marisaldi, M., Ursi, A., de Boer, A. I., Bardet, M., Allasia, C., Boissin, J. F., Flourens, F., and Østgaard, N.: In-Flight Observation of Gamma Ray Glows by ILDAS, Journal of Geophysical Research: Atmospheres, https://doi.org/10.1002/2017JD027405, 2017.

KronTechInc.: CHRONOS 1.4 DATASHEET, accessed 13 April 2022, https://www.krontech.ca/wp-content/uploads/2021/09/FM-ENGR-50001-Chronos-1.4-Datasheet-Rev5.pdf, 2021.

López, J. A., Pineda, N., Montanyà, J., Velde, O. v. d., Fabró, F., and Romero, D.: Spatio-temporal dimension of lightning flashes based on three-dimensional Lightning Mapping Array, Atmospheric research, 197, 255–264, https://doi.org/10.1016/j.atmosres.2017.06.030, 2017.

Mazur, V., Ruhnke, L. H., Warner, T. A., and Orville, R. E.: Recoil leader formation and development, Journal of Electrostatics, 71, 763–768, https://doi.org/https://doi.org/10.1016/j.elstat.2013.05.001, 2013.

McCarthy, M. and Parks, G. K.: Further observations of X-rays inside thunderstorms, Geophysical Research Letters, 12, 393–396, https://doi.org/10.1029/GL012i006p00393, 1985.

Michimoto, K.: Meteorological Aspects of Winter Thunderstorms along the Hokuriku Coast of Japan, IEEJ Transactions on Power and Energy, 127, 1242–1246, https://doi.org/10.1541/ieejpes.127.1242, 2007.

MLAB.cz: Barometric sensor with termometer WINDGAUGE03A, accessed 13 April 2022, https://mlab.cz/module/ALTIMET01A, 2015.

MLAB.cz: VLF antenna interconnection module, accessed 13 April 2022, https://github.com/mlab-modules/VLFANT01, 2017.

MLAB.cz: Venturi tube based anemometer WINDGAUGE03A, accessed 13 April 2022, https://www.mlab.cz/module/WINDGAUGE03A, 2020.

MLAB.cz: Electric Field mill interface module FIELDMILL01A, accessed 13 April 2022, https://www.mlab.cz/module/FIELDMILL01A, 2021.

Parks, G. K., Mauk, B. H., Spiger, R., and Chin, J.: X-ray enhancements detected during thunderstorm and lightning activities, Geophysical Research Letters, 8, 1176–1179, https://doi.org/10.1029/GL008i011p01176, 1981.

Rakov, V. A. and Kereszy, I.: Ground-based observations of lightning-related X-ray/gamma-ray emissions in Florida: Occurrence context and new insights, Electric Power Systems Research, 213, 108 736, https://doi.org/https://doi.org/10.1016/j.epsr.2022.108736, 2022.

Rakov, V. A. and Uman, M. A.: Lightning: Physics and Effects, Cambridge University Press, https://doi.org/10.1017/CBO9781107340886, 2003.

Rison, W., Thomas, R. J., Krehbiel, P. R., Hamlin, T., and Harlin, J.: A GPS-based three-dimensional lightning mapping system: Initial observations in central New Mexico, Geophysical Research Letters, 26, 3573–3576, https://doi.org/10.1029/1999GL010856, 1999.

Shi, F., Liu, N., Dwyer, J. R., and Ihaddadene, K. M. A.: VHF and UHF Electromagnetic Radiation Produced by Streamers in Lightning, Geophysical Research Letters, 46, 443–451, https://doi.org/https://doi.org/10.1029/2018GL080309, 2019.

Torii, T., Takeishi, M., and Hosono, T.: Observation of gamma-ray dose increase associated with winter thunderstorm and lightning activity, Journal of Geophysical Research: Atmospheres, 107, ACL 2–1–ACL 2–13, https://doi.org/10.1029/2001JD000938, 2002.

Tsuchiya, H., Enoto, T., Torii, T., Nakazawa, K., Yuasa, T., Torii, S., Fukuyama, T., Yamaguchi, T., Kato, H., Okano, M., Takita, M., and Makishima, K.: Observation of an energetic radiation burst from mountain-top thunderclouds., Physical Review Letters, 102, 255 003, https://doi.org/10.1103/PhysRevLett.102.255003, 2009.

UST.cz: Mobile piezoelectric distrometer DISTROMETER01A, accessed 13 April 2022, https://github.com/UniversalScientificTechnologies/DISTROMETER01, 2020.

UST.cz: UHF Radio Storm Monitoring Station, accessed 13 April 2022, https://github.com/UniversalScientificTechnologies/RSMS01, 2021.

Velychko, O., Ambrožová, I., Kákona, M., and Ploc, O.: CHARACTERISATION OF AIRDOS-C DETECTOR FOR MEASUREMENT OF HIGH-ENERGY EVENTS IN THE ATMOSPHERE, Radiation Protection Dosimetry, 198, 604–610, https://doi.org/10.1093/rpd/ncac105, 2022.

Wada, Y., Enoto, T., Nakazawa, K., Furuta, Y., Yuasa, T., Nakamura, Y., Morimoto, T., Matsumoto, T., Makishima, K., and Tsuchiya, H.: Downward Terrestrial Gamma-Ray Flash Observed in a Winter Thunderstorm, Phys. Rev. Lett., 123, 061 103, https://doi.org/10.1103/PhysRevLett.123.061103, 2019.

Windyty, S.: Accessed 13 April 2022, https://www.windy.com/, 2021.

Wu, T., Wang, D., and Takagi, N.: Lightning mapping with an array of fast antennas, Geophysical Research Letters, 45, 3698–3705, https://doi.org/10.1002/2018GL077628, 2018.

Østgaard, N., Neubert, T., Reglero, V., Ullaland, K., Yang, S., Genov, G., Marisaldi, M., Mezentsev, A., Kochkin, P., Lehtinen, N., Sarria, D., Qureshi, B. H., Solberg, A., Maiorana, C., Albrechtsen, K., Budtz-Jørgensen, C., Kuvvetli, I., Christiansen, F., Chanrion, O., Heumesser, M., and Al-nussirat, S.: First 10 months of TGF observations by ASIM, Journal of Geophysical Research: Atmospheres, 124, 14 024–14 036, https://doi.org/10.1029/2019JD031214, 2019.

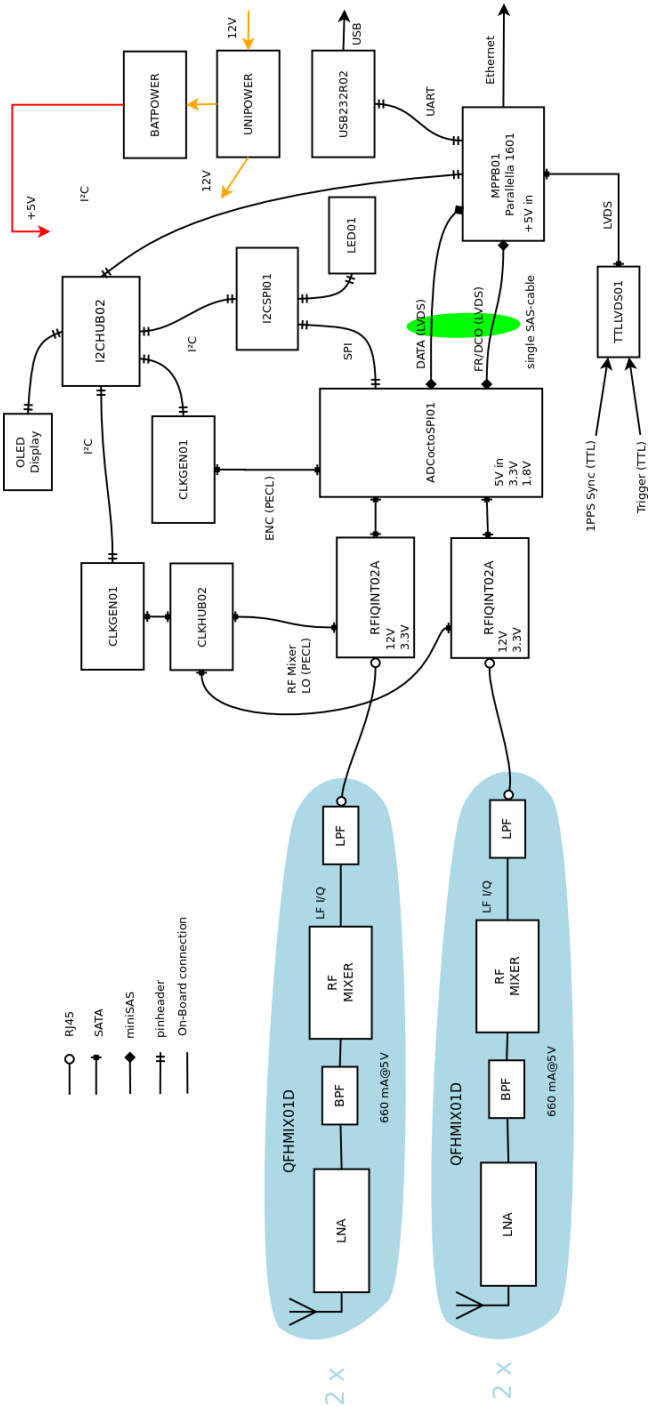

Figure A1. Block diagram of the UHF radio receiver used in the experiment. The internals of the active antenna mounted on the car roof is depicted in blue bubbles on the left of the schematics